Contribution from the Department of Chemistry, Rutgers, The State University of New Jersey, New Brunswick, New Jersey 08903

Thermally and Optically Driven Spin-State Transitions in $Fe(5,6\text{-dmp})_2(NCS)_2$ and Related Complexes and the Crystal Structure of $Fe(2,9\text{-dmp})_2(NCS)_2 \cdot {}^1/_4H_2O$

D. C. Figg, R. H. Herber,* and J. A. Potenza

Received July 3, 1990

$Fe(5,6\text{-dmp})_2(NCS)_2$, where dmp is dimethyl-1,10-phenanthroline, is shown to undergo a thermally driven spin-crossover transition using magnetic susceptibility and ^{57}Fe Mossbauer and infrared spectroscopy. The LIESST (light-induced excited spin-state trapping) phenomenon and related details of low-temperature spin-state conversions of this compound were studied using variable-temperature infrared spectroscopy. Evidence of low-temperature quantum mechanical tunneling from the "trapped" high-spin state to the low-spin state is reported for $Fe(5,6\text{-dmp})_2(NCS)_2$. The spin-state transitions of related methyl-substituted (phenanthroline)iron(II) complexes are briefly discussed. The single-crystal X-ray structure of the non-spin-crossover complex $Fe(2,9\text{-dmp})_2(NCS)_2 \cdot {}^1/_4H_2O$ is reported [triclinic, space group $P\bar{1}$, $Z = 2$, $a = 10.837$ (1) Å, $b = 14.811$ (1) Å, $c = 9.7782$ (9) Å, $\alpha = 101.511$ (8)°, $\beta = 109.909$ (9)°, $\gamma = 77.101$ (9)°, $R_F = 0.033$, $R_{wF} = 0.043$] and compared to that of the unsubstituted parent compound $Fe(phen)_2(NCS)_2$.

Introduction

The spin-crossover behavior of iron(II) complexes, involving transitions between high-spin (HS, $S = 2$, $^5T_{2g}$) and low-spin (LS, $S = 0$, $^1A_{1g}$) states, continues to be an actively studied phenomenon in transition-metal systems. Typically, the solid complex is in the HS form at ambient temperature and, with cooling, a spin-state conversion to the LS form occurs at some transition temperature T_1. Subsequent studies have revealed two types of spin-state transitions:[1] continuous (or gradual), which occur over a large temperature range, and discontinuous, which occur within a narrow temperature range. In 1984, Gutlich and co-workers[2] described a new optically-driven spin-state transition, termed light-induced excited spin-state trapping (LIESST), which has since been shown to occur in a number of solid Fe(II) spin-crossover complexes.[2-10] At temperatures below ~40 K, the thermally stable LS form can be converted to a "trapped HS" (HS_{tr}) form by irradiating the sample with light of the appropriate frequency. The LIESST process, and the presumed mechanism by which the complex becomes trapped in the HS form, have been described in detail.[3] In studies of a number of compounds reported to exhibit LIESST, the HS_{tr} form is observed to be stable for several days, if held at temperatures below ~40 K. On subsequent warming, the HS_{tr} form is thermally excited to permit passage over the classical energy barrier to the more stable LS form. Recently, data from this laboratory[11] as well as studies reported by Gutlich[8] have shown that, in some complexes which exhibit LIESST, the HS_{tr} form can quantum mechanically tunnel back to the LS form, at temperatures below ~25 K, when held in the dark.

Of the iron(II) systems, $Fe(phen)_2(NCS)_2$ (phen = 1,10-phenanthroline) is one of the most thoroughly studied spin-crossover complexes. In addition, the temperature-dependent behavior of the methyl-substituted phenanthroline complexes $Fe(4,7\text{-dmp})_2(NCS)_2$,[12,13] $Fe(2,9\text{-dmp})_2(NCS)_2$,[14] and $Fe(tmp)_2(NCS)_2$[15] (dmp = dimethyl-1,10-phenanthroline and tmp = 3,4,7,8-tetramethyl-1,10-phenanthroline) have previously been studied (the numbering scheme of phen is shown below).

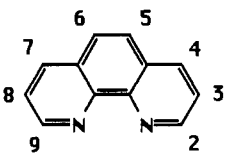

The remaining related, symmetrically-substituted dmp complexes, $Fe(5,6\text{-dmp})_2(NCS)_2$ and $Fe(3,8\text{-dmp})_2(NCS)_2$, have not been investigated in detail, although the pressure dependence of the spin state in $Fe(5,6\text{-dmp})_2(NCS)_2$ has been reported.[16a] As previously demonstrated, variable-temperature Fourier transform infrared (VTFTIR) spectroscopy can conveniently be used to follow the details of the thermally driven spin-crossover transition, as well as the optically driven LIESST phenomenon, in such complexes.[6,7,10] In the present study, VTFTIR and SQUID magnetic susceptibility data have been used to demonstrate the thermally-driven spin-state conversion in $Fe(5,6\text{-dmp})_2(NCS)_2$. The structure of the related compound $Fe(2,9\text{-dmp})_2(NCS)_2 \cdot {}^1/_4H_2O$ has been solved using single-crystal X-ray diffraction techniques. Data derived from this structure are used to account for its non-spin-crossover behavior. VTFTIR spectroscopy is used to demonstrate the LIESST phenomenon in $Fe(5,6\text{-dmp})_2(NCS)_2$ and to monitor related spin-state processes occurring at temperatures below 70 K.

Experimental Section

(a) Preparation of the Complexes. All syntheses were carried out under an atmosphere of argon or nitrogen.

$Fe(phen)_2(NCS)_2$ was synthesized as described previously.[6]

$Fe(5,6\text{-dmp})_2(NCS)_2$. The compound was obtained using the procedure previously described[17] to make the red "tris" 5,6-dmp, thiocyanate complex, which was then refluxed in a small amount of α-picoline. The product is violet and was characterized by elemental analysis (Anal. Calcd for $FeC_{30}H_{24}N_6S_2$: C, 61.2; H, 4.1; N, 14.3. Found: C, 61.1; H, 4.2; N, 14.2), SQUID magnetic susceptibility, ^{57}Fe Mossbauer spec-

(1) Konig, E.; Ritter, G.; Kulshreshtha, S. K. *Chem. Rev.* **1985**, *85*, 219.
(2) Decurtins, S.; Gutlich, P.; Kohler, C. P.; Spiering, H. *Chem. Phys. Lett.* **1984**, *105*, 1.
(3) Decurtins, S.; Gutlich, P.; Hasselbach, K. M.; Hauser, A.; Spiering, H. *Inorg. Chem.* **1985**, *24*, 2174.
(4) Decurtins, S.; Gutlich, P.; Kohler, C. P.; Spiering, H. *J. Chem. Soc., Chem. Commun.* **1985**, 430.
(5) Poganuich, P.; Gutlich, P. *Inorg. Chem.* **1987**, *26*, 455.
(6) Herber, R. H.; Casson, L. M. *Inorg. Chem.* **1986**, *25*, 847.
(7) Herber, R. H. *Inorg. Chem.* **1987**, *26*, 173.
(8) Adler, P.; Hauser, A.; Vef, A.; Spiering, H.; Gutlich, P. *Hyperfine Interact.* **1989**, *47*, 343.
(9) Hauser, A.; Gutlich, P.; Spiering, H. *Inorg. Chem.* **1986**, *25*, 4245.
(10) Figg, D. C.; Herber, R. H. *Inorg. Chem.* **1990**, *29*, 2170.
(11) (a) Figg, D. C.; Herber, R. H. *Time-Resolved Vibrational Spectroscopy*, Proceedings of the 4th International Conference, Princeton University, Princeton, NJ, June 11-16, 1989; Academic: New York, 1989; p 40. (b) Figg, D. C.; Herber, R. H. 1989 Mid-Atlantic Regional ACS Meeting, Cherry Hill, NJ, May 24-26, 1989; Inorg. Div. No. 96.
(12) (a) Konig, E.; Ritter, G.; Zimmermann, R. *Chem. Phys. Lett.* **1974**, *26*, 425. (b) Konig, E.; Ritter, G.; Kanellakopulos, B. *J. Phys. C* **1974**, *7*, 2681. (c) Konig, E.; Ritter, G. *Solid State Commun.* **1976**, *18*, 279. (d) Konig, E.; Ritter, G.; Madeja, K.; Bohmer, W. H. *Ber. Bunsen-Ges. Phys. Chem.* **1973**, *77*, 390.
(13) Figg, D. C. Ph.D. Thesis, Rutgers University, 1990.
(14) (a) Dockum, B. R.; Reiff, W. M. *Inorg. Chim. Acta* **1979**, *35*, 285. (b) Konig, E.; Ritter, G.; Madeja, K. *J. Inorg. Nucl. Chem.* **1981**, *43*, 2273.
(15) Cunningham, A. J.; Fergusson, J. E.; Powell, H. K.; Sinn, E.; Wong, H. *J. Chem. Soc., Dalton Trans.* **1972**, 2155.
(16) (a) Bargeron, C. B.; Drickamer, H. G. *J. Chem. Phys.* **1971**, *55*, 3471. (b) Fisher, D. C.; Drickamer, H. G. *J. Chem. Phys.* **1971**, *54*, 4825.
(17) Ganguli, P.; Gutlich, P.; Muller, E. W.; Irler, W. *J. Chem. Soc., Dalton Trans.* **1981**, 441.

0020-1669/92/1331-2111$03.00/0

Table I. Crystallographic Data for $Fe(2,9\text{-dmp})_2(NCS)_2 \cdot {}^1/_4H_2O$[a]

$FeS_2N_6C_{30}O_{0.5}H_{25}$	fw = 593.04
space group: $P\bar{1}$	$Z = 2$
temp = 296 (1) K	V = 1425 (2) Å^3
a = 10.837 (1) Å	α = 101.511 (8)°
b = 14.811 (1) Å	β = 109.909 (9)°
c = 9.7782 (9) Å	γ = 77.101 (9)°
d_{obsd} = 1.37 (1) g·cm^{-3}	d_{calcd} = 1.382 g·cm^{-3}
λ = 0.71073 Å	linear abs coeff = 7.0 cm^{-1}
R_F = 0.033	R_{wF} = 0.043

[a] $R_F = \sum||F_o| - |F_c||/\sum|F_o|$. $R_{wF} = [\sum(|F_o| - |F_c|)^2/\sum w|F_o|^2]^{1/2}$.

troscopy, and VTFTIR spectroscopy.

$Fe(2,9\text{-dmp})_2(NCS)_2 \cdot {}^1/_4H_2O$. Single crystals were grown on a Teflon anion-permeable membrane in a two-compartment cell.[18] $FeCl_2 \cdot 4H_2O$ (1 mmol) and 2,9-dmp (1.9 mmol) were dissolved in 15 mL of a 30% H_2O/70% ethanol solution and placed on one side of the membrane; the other compartment was filled with a solution of NaSCN (2.4 mmol) in 15 mL of H_2O. The system was closed and maintained for several days until crystals formed on the membrane. The crystals were removed, washed with H_2O, and vacuum-dried. These crystals or microcrystalline powders obtained from them were used in all subsequent experiments. Single-crystal X-ray analysis revealed a disordered water molecule on a partially occupied site and gave the empirical formula as $Fe(2,9\text{-dmp})_2(NCS)_2 \cdot {}^1/_4H_2O$. Despite the disorder and the possibility that drying partially removed the solvent molecule, the structure refined well, as determined by the standard measures (see below). Anal. Calcd for $FeC_{30}H_{24.5}N_6O_{0.25}S_2$: C, 60.8; H, 4.2; N, 14.2. Found: C, 61.1; H, 3.8; N, 14.0.

$Fe(tmp)_2(NCS)_2$. This compound was synthesized by the method used for $Fe(5,6\text{-dmp})_2(NCS)_2$, employing α-picoline as the reflux solvent. The red product was characterized by elemental analysis (Anal. Calcd for $FeC_{34}H_{32}N_6S_2$: C, 63.4; H, 5.0; N, 13.0. Found: C, 63.0; H, 4.9; N, 12.9) and VTFTIR spectroscopy.

(b) Magnetic Studies. Variable-temperature magnetic data for $Fe(5,6\text{-dmp})_2(NCS)_2$ were collected using a SQUID magnetic susceptometer (Quantum Design, Inc.) which had been calibrated against an NBS Pd standard. The sample was held in a Lilly No. 5 clear gelatin capsule for data collection. The field strength was 1000 G. Effective magnetic moments were calculated as $\mu_{eff} = 2.828(\chi_m T)^{1/2}$, where χ_m is the corrected molar susceptibility. Diamagnetic corrections were made for the sample holder, and a value of $-377\ 10^{-6}$ cm^3·mol^{-1} was used as the diamagnetic correction for the complex.[12d] The inflection point of the plot of μ_{eff} vs T was used to estimate T_1.

(c) X-ray Diffraction Studies. An orange needle of $Fe(2,9\text{-dmp})_2(NCS)_2 \cdot {}^1/_4H_2O$ was mounted on the end of a glass rod. Diffraction measurements were made with an Enraf-Nonius CAD-4 diffractometer using graphite-monochromated Mo Kα radiation. The Enraf-Nonius Structure Determination Package[19] was used for data collection, data processing, and structure solution. Diffractometer examination of the reciprocal lattice revealed a triclinic system with no systematic absences. The structure was solved and refined successfully in space group $P\bar{1}$. Crystal data and additional details regarding data collection and refinement are presented in Table I and in the supplementary material. Intensity data were collected and corrected for decay, absorption (empirical, ψ-scan), and Lp effects.

The structure was solved by direct methods and refined on F with full-matrix least-squares techniques. An E map, based on 392 phases ($|E| > 1.352$), from the starting set having the highest combined figure of merit revealed coordinates for Fe, the NCS ligands, and several atoms from the dimethylphenanthroline ligands. The remaining non-H atoms were located from successive difference Fourier maps. Following anisotropic refinement, all ligand H atoms were located on a difference map and their coordinates were subsequently refined. H atom temperature factors were set according to $B_H = 1.3B_N$, where N is the atom bonded to H. Refinement, with all non-H atoms anisotropic, led to convergence with $R_F = 0.038$, $R_{wF} = 0.051$, and GOF = 1.68. A difference map at this point showed a peak of 0.67 e·A^{-3} near the origin (0, 0, 1) which was significantly larger than the highest negative peak and which was well-removed from the remaining atoms. It was assumed that this peak arose from the O atom of a water molecule of solvation on a partially occupied site. Inclusion of an O atom with a multiplier of 0.25 led to a significant reduction in R_F and R_{wF}. Several cycles of refinement (including isotropic refinement of the O atom) led to convergence with $R_F = 0.033$, $R_{wF} = 0.043$, and GOF = 1.41. Attempts to increase the atom multiplier of O increased R_{wF} and gave unrealistically high temperature factors for oxygen. We conclude that the stoichiometry of the crystal used to collect data is given by $Fe(2,9\text{-dmp})_2(NCS)_2 \cdot {}^1/_4H_2O$ within experimental error. A final difference map showed no significant features; the highest positive peak (0.26 e·A^{-3}) was only marginally larger than the highest negative peak (−0.20 e·A^{-3}). A view of the complex, showing the atom-numbering

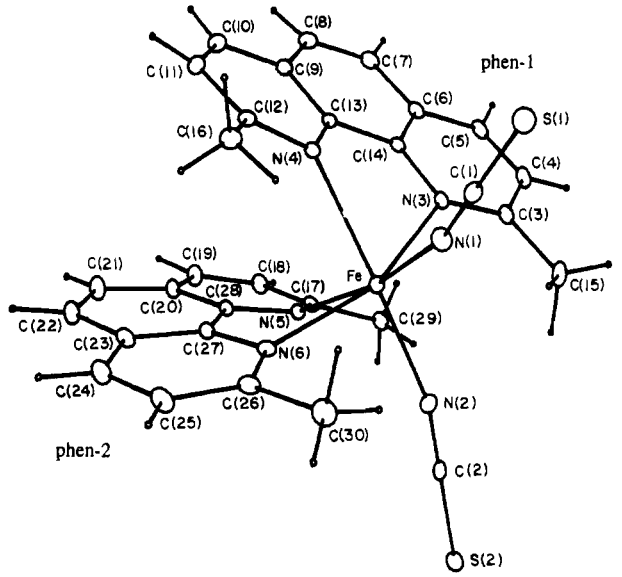

Figure 1. ORTEP view of $Fe(2,9\text{-dmp})_2(NCS)_2$, showing the atom-numbering scheme.

Table II. Fractional Atomic Coordinates and Equivalent Isotropic Thermal Parameters for $Fe(2,9\text{-dmp})_2(NCS)_2 \cdot {}^1/_4H_2O$[a]

atom	x	y	z	B_{eq}, Å^2
Fe	0.27271 (4)	0.25242 (3)	0.68774 (5)	3.47 (1)
S(1)	−0.1245 (1)	0.25641 (8)	0.8045 (1)	5.83 (3)
S(2)	0.6925 (1)	0.18529 (7)	1.0554 (1)	5.06 (3)
N(1)	0.1202 (3)	0.2455 (2)	0.7635 (3)	5.35 (8)
N(2)	0.4347 (3)	0.2281 (2)	0.8730 (3)	5.01 (9)
N(3)	0.2297 (2)	0.4085 (2)	0.7166 (3)	3.52 (7)
N(4)	0.1231 (2)	0.2956 (2)	0.4702 (3)	3.36 (7)
N(5)	0.4189 (2)	0.2565 (2)	0.5618 (3)	3.11 (6)
N(6)	0.3164 (3)	0.1082 (2)	0.5737 (3)	3.81 (7)
C(1)	0.0185 (3)	0.2494 (2)	0.7796 (4)	4.10 (9)
C(2)	0.5424 (3)	0.2106 (2)	0.9487 (3)	3.55 (8)
C(3)	0.2630 (3)	0.4679 (3)	0.8407 (4)	4.4 (1)
C(4)	0.2687 (4)	0.5608 (3)	0.8369 (4)	5.2 (1)
C(5)	0.2404 (4)	0.5928 (3)	0.7079 (4)	5.0 (1)
C(6)	0.1998 (3)	0.5341 (2)	0.5757 (4)	4.05 (9)
C(7)	0.1649 (4)	0.5623 (3)	0.4350 (4)	5.1 (1)
C(8)	0.1217 (4)	0.5037 (3)	0.3111 (4)	5.0 (1)
C(9)	0.1074 (3)	0.4114 (3)	0.3178 (4)	3.97 (9)
C(10)	0.0560 (4)	0.3491 (3)	0.1940 (4)	5.0 (1)
C(11)	0.0297 (4)	0.2663 (3)	0.2095 (4)	5.0 (1)
C(12)	0.0600 (3)	0.2423 (3)	0.3505 (4)	4.03 (9)
C(13)	0.1418 (3)	0.3802 (2)	0.4542 (3)	3.23 (8)
C(14)	0.1938 (3)	0.4420 (2)	0.5861 (3)	3.33 (8)
C(15)	0.2937 (5)	0.4325 (3)	0.9827 (4)	6.4 (1)
C(16)	0.0158 (4)	0.1587 (3)	0.3712 (5)	5.3 (1)
C(17)	0.4819 (3)	0.3245 (2)	0.5633 (4)	3.63 (9)
C(18)	0.5101 (3)	0.3352 (3)	0.4384 (4)	4.6 (1)
C(19)	0.4813 (4)	0.2731 (3)	0.3155 (4)	5.0 (1)
C(20)	0.4255 (3)	0.1960 (3)	0.3147 (4)	4.08 (9)
C(21)	0.4037 (4)	0.1230 (3)	0.1956 (4)	5.8 (1)
C(22)	0.3646 (4)	0.0451 (3)	0.2060 (4)	5.6 (1)
C(23)	0.3396 (4)	0.0356 (2)	0.3345 (4)	4.6 (1)
C(24)	0.3037 (4)	−0.0452 (3)	0.3538 (5)	5.7 (1)
C(25)	0.2816 (4)	−0.0496 (3)	0.4802 (5)	5.9 (1)
C(26)	0.2864 (3)	0.0290 (2)	0.5908 (4)	4.7 (1)
C(27)	0.3482 (3)	0.1100 (2)	0.4510 (4)	3.44 (8)
C(28)	0.3962 (3)	0.1900 (2)	0.4412 (3)	3.23 (8)
C(29)	0.5268 (3)	0.3883 (3)	0.7037 (4)	4.6 (1)
C(30)	0.2579 (4)	0.0273 (3)	0.7289 (5)	6.6 (1)

[a] $B_{eq} = 4(\sum_i\sum_j \beta_{ij} a_i a_j)/3$.

(18) Bino, A. Private communication.
(19) *Enraf-Nonius Structure Determination Package*; Enraf-Nonius: Delft, Holland, 1985.

Table III. Selected Interatomic Distances (Å) and Angles (deg) for $Fe(2,9\text{-dmp})_2(NCS)_2 \cdot {}^1/_4H_2O$

Coordination Sphere											
Fe–N(1)	2.058 (3)	Fe–N(3)	2.233 (3)	Fe–N(5)	2.331 (2)	Fe–N(2)	2.076 (3)	Fe–N(4)	2.301 (2)	Fe–N(6)	2.233 (3)
N(1)–Fe–N(2)	100.3 (1)	N(1)–Fe–N(3)	92.0 (2)	N(1)–Fe–N(4)	91.0 (2)						
N(1)–Fe–N(5)	170.1 (2)	N(1)–Fe–N(6)	103.4 (1)	N(2)–Fe–N(3)	101.2 (2)						
N(2)–Fe–N(4)	167.5 (2)	N(2)–Fe–N(5)	89.1 (2)	N(2)–Fe–N(6)	92.8 (2)						
N(3)–Fe–N(4)	73.11 (9)	N(3)–Fe–N(5)	89.13 (9)	N(3)–Fe–N(6)	157.1 (1)						
N(4)–Fe–N(5)	79.86 (8)	N(4)–Fe–N(6)	89.51 (9)	N(5)–Fe–N(6)	72.8 (1)						
NCS Ligands											
S(1)–C(1)	1.628 (4)	S(2)–C(2)	1.614 (4)	S(1)–C(1)–N(1)	179.1 (3)	S(2)–C(2)–N(2)	179.3 (3)				
N(1)–C(1)	1.153 (5)	N(2)–C(2)	1.153 (5)	Fe–N(1)–C(1)	165.7 (3)	Fe–N(2)–C(2)	161.7 (3)				
2,9-dmp											
N(3)–C(3)	1.341 (5)	N(6)–C(26)	1.341 (5)	C(8)–C(9)	1.426 (5)	C(20)–C(21)	1.417 (5)				
C(3)–C(4)	1.399 (5)	C(25)–C(26)	1.420 (5)	C(9)–C(10)	1.398 (6)	C(19)–C(20)	1.404 (5)				
C(3)–C(15)	1.487 (6)	C(26)–C(30)	1.490 (6)	C(9)–C(13)	1.401 (4)	C(20)–C(28)	1.401 (4)				
C(4)–C(5)	1.349 (5)	C(24)–C(25)	1.353 (6)	C(10)–C(11)	1.368 (5)	C(18)–C(19)	1.350 (6)				
C(5)–C(6)	1.398 (6)	C(23)–C(24)	1.403 (5)	C(11)–C(12)	1.404 (5)	C(17)–C(18)	1.400 (5)				
C(6)–C(14)	1.405 (4)	C(23)–C(27)	1.413 (4)	C(12)–C(16)	1.495 (5)	C(17)–C(29)	1.500 (5)				
N(3)–C(14)	1.362 (4)	N(6)–C(27)	1.362 (4)	C(13)–C(14)	1.444 (4)	C(27)–C(28)	1.427 (4)				
C(6)–C(7)	1.420 (6)	C(22)–C(23)	1.412 (5)	N(4)–C(12)	1.338 (4)	N(5)–C(17)	1.333 (4)				
C(7)–C(8)	1.348 (6)	C(21)–C(22)	1.347 (6)	N(4)–C(13)	1.359 (4)	N(5)–C(28)	1.367 (4)				
Dihedral Angle											
phen-1/phen-2	153.52 (8)										
Methyl Carbons Intramolecular Contacts <4 Å											
C(16)···N(6)	3.196 (4)	C(29)···N(3)	3.211 (5)	C(16)···C(25)	3.770 (5)	C(29)···C(4)	3.743 (5)				
C(16)···C(23)	3.676 (5)	C(29)···C(6)	3.665 (4)	C(16)···C(26)	3.428 (5)	C(29)···C(3)	3.440 (6)				
C(16)···C(24)	3.852 (5)	C(29)···C(5)	3.827 (5)	C(16)···C(27)	3.357 (5)	C(29)···C(14)	3.353 (4)				
Torsion Angles											
N(4)–Fe–N(3)–C(14)	−27.2 (2)	N(5)–Fe–N(6)–C(27)	−27.4 (2)	Fe–N(4)–C(13)–C(14)	−28.1 (4)	Fe–N(5)–C(28)–C(27)	−29.0 (3)				
N(3)–Fe–N(4)–C(13)	29.1 (2)	N(6)–Fe–N(5)–C(28)	29.6 (2)	N(4)–C(13)–C(14)–N(3)	4.8 (5)	N(5)–C(28)–C(27)–N(6)	5.9 (5)				
Fe–N(3)–C(14)–C(13)	22.5 (4)	Fe–N(6)–C(27)–C(28)	22.4 (4)								

scheme, is given in Figure 1, and the non-H fractional atomic coordinates are listed in Table II.

(d) Variable-Temperature Infrared Spectroscopy. Changes in the CN stretching modes of the NCS ligands in these complexes were used as previously described[6,7] to follow the thermal conversion between the HS and LS forms, as well as the details of the LIESST process. All VTFTIR and LIESST measurements were carried out on neat samples, dispersed in Kel-F mulls to minimize effects due to crushing and pelletizing.[7,20,21] Typically, 100 sample scans at 2-cm^{-1} resolution were coadded and normalized to data for a KBr blank at room temperature. All other techniques and instrumentation used were as described previously,[6,7,22] including the use of a blue filter during LIESST experiments.

(e) ^{57}Fe Mossbauer Spectroscopy. γ-Ray resonance spectra were obtained at 90 and 295 K for $Fe(5,6\text{-dmp})_2(NCS)_2$ and $Fe(tmp)_2(NCS)_2$, using a standard, constant-acceleration spectrometer calibrated with 0.5 mil of iron at room temperature. In a typical experiment, a neat microcrystalline powder sample, containing ca. 1.8×10^{17} ^{57}Fe atoms/cm^2, was layered in a plastic sample holder and examined in transmission. Assuming a recoil-free fraction at 90 K of ca. 0.7 leads to an optical thickness of ca. 0.32; hence no thickness corrections were applied to the results. To reduce random noise, in excess of 10^6 counts/channel were scaled at both 90 and 295 K, using a 100 mCi ^{57}Co(Rh) source at room temperature, in conjunction with a Harwell fast proportional counter. All isomer shifts are reported with respect to the centroid of the four inner lines of a room temperature Fe(0) transmission spectrum.

Results and Discussion

(a) Magnetic Studies. The temperature dependence of μ_{eff} of $Fe(5,6\text{-dmp})_2(NCS)_2$ on warming is shown in Figure 2. The effective moments at 100 K (0.50 μ_B) and 353 K (4.88 μ_B) are consistent with singlet and quintet states, respectively. It is likely that cooling or warming beyond the temperature range used for this study would show further conversion since the end point μ_{eff} values calculated are not temperature-independent values. The spin-state transition appears to be the continuous type since it occurs over a temperature range greater than 100 deg. The T_1 value obtained from the SQUID magnetic data is 221 K.

On the basis of the electron-donating character of a methyl substituent and on redox potentials,[23] all of the methyl-substituted phenanthroline ligands should yield slightly stronger ligand fields at the metal center than phenanthroline. On this basis alone, the HS ⇔ LS transition in the methylated complexes should occur at T_1 values higher than that for $Fe(phen)_2(NCS)_2$. The only compound for which this is true is $Fe(5,6\text{-dmp})_2(NCS)_2$. $Fe(4,7\text{-dmp})_2(NCS)_2$[12] has a T_1 value lower than that of $Fe(phen)_2(NCS)_2$, while $Fe(2,9\text{-dmp})_2(NCS)_2$ and $Fe(tmp)_2(NCS)_2$ do not show crossover behavior down to 6 K.

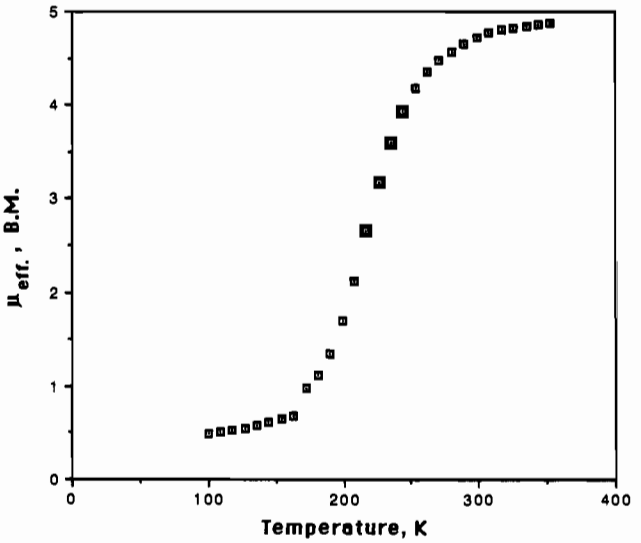

Figure 2. Effective magnetic moment of $Fe(5,6\text{-dmp})_2(NCS)_2$ as a function of temperature on warming.

(b) $Fe(2,9\text{-dmp})_2(NCS)_2 \cdot {}^1/_4H_2O$ Crystal Structure. The crystal structure of $Fe(2,9\text{-dmp})_2(NCS)_2$ was determined so that the structural features which inhibit spin-state conversion could be carefully examined. The structure of $Fe(2,9\text{-dmp})_2(NCS)_2$ (Figure 1) contains neutral molecules separated by the disordered solvate molecules. Table III lists selected bond lengths and angles.

(20) Muller, E. W.; Spiering, H.; Gutlich, P. *J. Chem. Phys.* **1983**, *79*, 1439.
(21) Muller, E. W.; Spiering, H.; Gutlich, P. *Chem. Phys. Lett.* **1982**, *93*, 567.
(22) Casson, L. M.; Herber, R. H. *Rev. Sci. Instrum.* **1985**, *56*, 1593.
(23) The G. Frederick Smith Chemical Co. catalog (1988) contains a compilation of the redox potentials of the tris ferrous complexes.

Recently, the crystal structure of the parent spin-crossover complex, $Fe(phen)_2(NCS)_2$, was reported both for its HS and LS form (space group = *Pbcn* for both forms)[24] and therefore comparisons between the HS form of the phen and the non-spin-crossover 2,9-dmp complex can be made.

Each Fe is bonded to four N atoms from two 2,9-dmp ligands and the N atoms of two thiocyanate ligands. The coordination geometry is distorted cis octahedral. In the 2,9-dmp complex, distortions from octahedral geometry are somewhat greater than in the phen complex, as judged by the trans N–Fe–N angles. Deviations of the iron atom from the least-squares planes formed from the three possible sets of equatorial N atoms (e.g. N(1), N(2), N(4), and N(5), etc.) are 0.019 (3), −0.241 (3), and −0.272 (1) Å in the 2,9-dmp complex and 0.000 (1), 0.163 (1), and −0.163 (1) Å in the phen complex. The plane from which the iron atom deviates the least in both complexes is that which contains both NCS nitrogens. The mean bite angle of the two 2,9-dmp ligands is 73.0 (2)°, on the low side of the range observed for related HS bis(NCS), bis(N-donor) bidentate complexes: 76.1 (1)° for $Fe(phen)_2(NCS)_2$, 75 (1)° for $Fe(bpy)_2(NCS)_2$,[25] and 73.8 (4)° for $Fe(bt)_2(NCS)_2$,[26] all at room temperature. Significantly larger values have been reported for LS complexes; 81.8 (1)° for $Fe(phen)_2(NCS)_2$ at 130 K, 80 (1)° for $Fe(bpy)_2(NCS)_2$ at 100 K, and 82.9 (3)° for a LS unsubstituted tris(phenanthroline) ferrous complex at room temperature.[27] The larger bite angles in the LS complexes are probably a result of their shorter Fe–N bond lengths.

Of greater interest are the Fe–N distances, since these are related to the crystal field strength, and hence the spin behavior of the iron d-electrons. The $Fe–N_{CS}$ distances in $Fe(2,9\text{-}dmp)_2(NCS)_2 \cdot {}^1/_4H_2O$ average 2.067 (13) Å, equal to the value [$Fe–N_{CS}$ average value, 2.07 (1) Å] found in the related HS complexes $Fe(phen)_2(NCS)_2$, $Fe(bpy)_2(NCS)_2$, and $Fe(bt)_2(NCS)_2$, all at room temperature. These data, along with the bite angles discussed above, suggest that the NCS ligands in the 2,9-dmp complex are not sterically crowded by the methyl groups and assume a geometry governed primarily by bonding considerations. The $Fe–N_{2,9\text{-}dmp}$ distances average 2.27 (5) Å. This is the longest average for Fe–N bonds reported for an iron(II) complex containing bidentate N-donor ligands of which we are aware.[24-26,28,29] The $Fe–N_{phen}$ distances in the HS form of $Fe(phen)_2(NCS)_2$ (293 K) average 2.205 (8) Å, similar to values obtained for other iron(II) HS complexes which do undergo a thermally-driven spin-state transition to the LS form on cooling. The longer bond distance between the metal atom and the bidentate ligand, compared to the unsubstituted parent complex, leads to a weakening of the crystal field, consistent with the failure of $Fe(2,9\text{-}dmp)_2(NCS)_2 \cdot {}^1/_4H_2O$ to undergo a HS → LS transition down to 6 K.

Detailed examination of the structure yields a plausible reason as to why the $Fe–N_{2,9\text{-}dmp}$ bond distances are as observed. The two methyl groups [C(16) and C(29), one from each 2,9-dmp ligand] trans to the SCN ligands are sterically crowded. C(16) shows six intramolecular contacts <4 Å with phen-2 (Figure 1 defines phen-1 and phen-2), as does C(29) with phen-1 (see Table III). The other two methyl carbons, C(15) and C(30), show no such contacts. Distortions caused by the steric crowding of C(16) and C(29) are also apparent from the planarity of the 2,9-dmp ligands. Each ligand is somewhat bowed, with the largest deviation from the calculated planes being 0.162 (4) Å (as compared to 0.039 (3) Å in the phen ligands of the parent complex). The sterically crowded carbons [C(16) and C(29)] deviate from the ligand planes by almost 0.5 Å whereas the two other methyl carbons deviate less than 0.04 Å from the calculated planes. Both C(16) and C(29) deviate in a direction away from the other dmp ligand. A result of this steric crowding is that N(4) and N(5) are not able to get as close to Fe as N(3) and N(6), as shown by the bond distances in Table III. Another apparent result of steric crowding is that the dihedral angle between the two 2,9-dmp ligands is 153.5 (1)°, quite different from that observed in $Fe(phen)_2(NCS)_2$ [86.9 (1)°]. A result of the 2,9-dmp ligands bending away from each other is that the iron atom deviates 1.004 (1) Å from the plane of phen-1 and 1.071 (1) Å from the plane of phen-2. The deviation of Fe from the 2,9-dmp planes is such that the five-membered chelate rings adopt the envelope configuration as indicated by the torsion angles in Table III. This compares to an approximately planar configuration between Fe and the phen ligands in $Fe(phen)_2(NCS)_2$, with Fe deviating only 0.077 Å from each ligand plane. This suggests that π-back-donation from the 2,9-dmp ligands to iron should be significantly reduced compared with the unsubstituted complex. This in turn

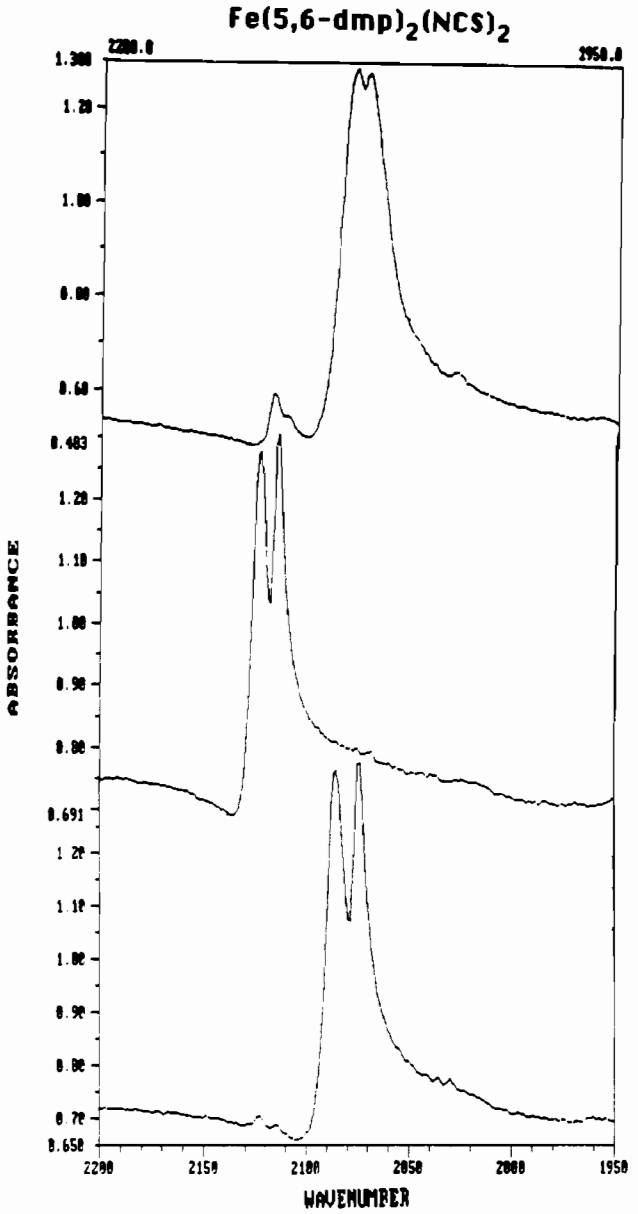

Figure 3. Portion of the IR absorption spectrum (2200–1950 cm^{-1}) of $Fe(5,6\text{-}dmp)_2(NCS)_2$ showing the CN stretching modes of the HS form at 298.5 K (a, top), LS form at 6 K (b, center), HS_{tr} form at 6 K (c, bottom).

(24) Gallois, B.; Real, J.-A.; Hauw, C.; Zarembowitch, J. *Inorg. Chem.* **1990**, *29*, 1152.
(25) Konig, E.; Watson, K. *Chem. Phys. Lett.* **1970**, *6*, 457.
(26) Ozarowski, A.; McGarvey, B. R.; Sarkar, H. B.; Drake, J. E. *Inorg. Chem.* **1988**, *27*, 628.
(27) Zalkin, A.; Templeton, D. H.; Ueki, T. *Inorg. Chem.* **1973**, *12*, 1641.
(28) Johansson, L.; Molund, M.; Oskarsson, A. *Inorg. Chim. Acta* **1978**, *31*, 117. Baker, A. T.; Goodwin, H. A.; Rae, A. D. *Inorg. Chem.* **1987**, *26*, 3513. Wiehl, L.; Kiel, G.; Kohler, C. P.; Spiering, H.; Gutlich, P. *Inorg. Chem.* **1986**, *25*, 1565. Katz, B. A.; Strouse, C. E. *Inorg. Chem.* **1980**, *19*, 658. Mikami, M.; Konno, M.; Saito, Y. *Acta Crystallogr.* **1980**, *B36*, 275. Katz, B. A.; Strouse, C. E. *J. Am. Chem. Soc.* **1979**, *101*, 6214.
(29) Goodwin, H. A.; Kucharski, E. S.; White, A. H. *Aust. J. Chem.* **1983**, *36*, 1115.

Table IV. Frequency of the CN Stretching Modes in the HS and LS States

compd	HS, cm^{-1} (temp, K)	LS, cm^{-1} (temp, K)	HS_{tr}, cm^{-1} (temp, K)
$Fe(phen)_2(NCS)_2$	2074, 2062 (303)	2114, 2107 (80)	2075, 2062 (6)
$Fe(4,7\text{-dmp})_2(NCS)_2$	2084, 2058 (296)	2129, 2104 (67)	2081, 2061 (7.5)
$Fe(5,6\text{-dmp})_2(NCS)_2$	2078, 2072 (298.5)	2122, 2114 (81)	2085, 2074 (6)
$Fe(2,9\text{-dmp})_2(NCS)_2$	2079 (s), 2070 (303)		
	2087, 2076 (6.5)		
$Fe(tmp)_2(NCS)_2$	2080, 2066 (296)		
	2088, 2074 (6.5)		

Table V. ^{57}Fe Mossbauer Parameters

	HS			LS			
complex	ΔE_q, $mm\cdot s^{-1}$	δ^{IS}, $mm\cdot s^{-1}$	temp, K	ΔE_q, $mm\cdot s^{-1}$	δ^{IS}, $mm\cdot s^{-1}$	temp, K	ref
$Fe(phen)_2(NCS)_2$	2.67	0.98	293	0.34	0.37	77	35
$Fe(4,7\text{-dmp})_2(NCS)_2$	2.56	0.98	298	0.47	0.32	4.2	16a, 12
$Fe(5,6\text{-dmp})_2(NCS)_2$	2.77	0.97	295	0.44	0.40	90	this study
	2.68	0.95	rt				16a
$Fe(2,9\text{-dmp})_2(NCS)_2\cdot{}^1/_4H_2O$	1.21	1.03	298				
	1.57	1.05	77				14b
	1.24	1.03	300				
	1.56	1.15	78				
	1.68	1.18	4.2				14a
$Fe(tmp)_2(NCS)_2$	2.80	0.98	295				
	3.27	1.07	90				this study

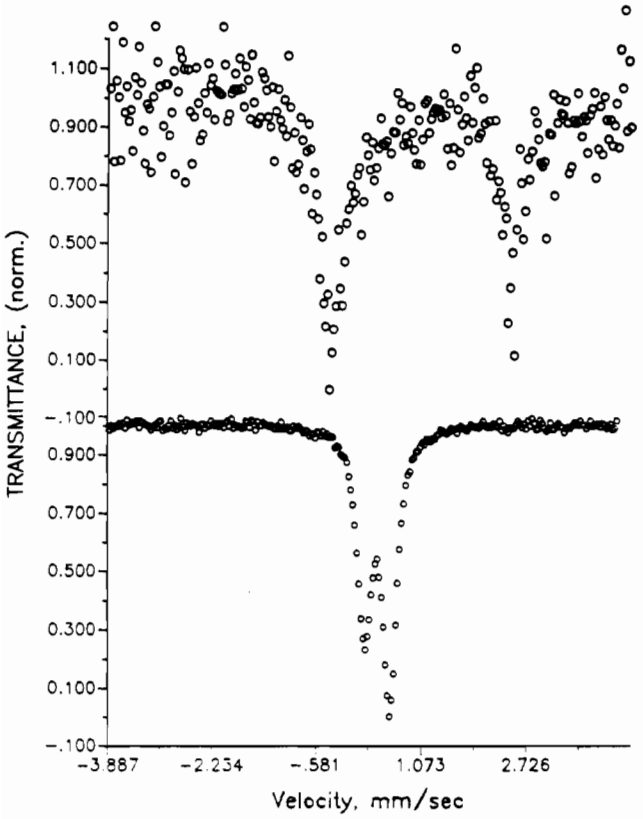

Figure 4. ^{57}Fe Mossbauer spectra of $Fe(5,6\text{-dmp})_2(NCS)_2$ at 295 K (a, top) and 90 K (b, bottom).

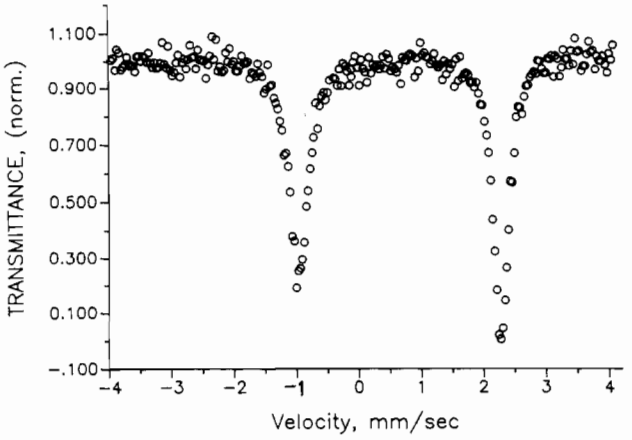

Figure 5. ^{57}Fe Mossbauer spectra of $Fe(tmp)_2(NCS)_2$ at 90 K.

may explain why the Fe–N(3) and Fe–N(6) bonds are not shorter.

(c) Variable-Temperature FTIR Studies. Details of the spin-state temperature dependence and the LIESST phenomenon will be discussed in terms of changes in the CN stretching modes of the NCS ligands. More detailed data for $Fe(phen)_2(NCS)_2$ and $Fe(4,7\text{-dmp})_2(NCS)_2$ are reported elsewhere.[6,7,13] The ν_{CN} region of $Fe(5,6\text{-dmp})_2(NCS)_2$ at 298.5 K (Figure 3a) shows very strong HS absorption bands at 2078 and 2072 cm^{-1} and a single, weaker LS band at 2116 cm^{-1} with a shoulder at ~2110 cm^{-1}. The ^{13}C component of the 2072-cm^{-1} band is seen at 2028 cm^{-1}. Splitting of the HS and LS bands arises from symmetric and asymmetric ν_{CN} modes, both of which are IR active in the cis NCS complexes. Similar IR signatures[7,10] have been observed for $Fe(phen)_2(NCS)_2$, $Fe(2,9\text{-dmp})_2(NCS)_2\cdot{}^1/_4H_2O$, $Fe(bpy)_2(NCS)_2$, and $Fe(bt)_2(NCS)_2$, for which the crystallographic data[24-26] show unambiguously the cis nature of the two pseudohalide ligands, and therefore the ν_{CN} splitting is taken as strong evidence for similar coordination geometries in the other complexes examined herein. The percentage of the HS form in $Fe(5,6\text{-dmp})_2(NCS)_2$ at 298.5 K (89%), as reflected in the IR data, agrees reasonably well with that calculated using magnetic susceptibility data (94% HS) at 297 K.

The temperature dependence of the spin-state conversion in $Fe(5,6\text{-dmp})_2(NCS)_2$ was followed using VTFTIR methods. The spin-state transition curve obtained by VTFTIR spectroscopy for $Fe(5,6\text{-dmp})_2(NCS)_2$ reproduces the shape and slope of the curve from magnetic measurements. The T_1 value obtained for both warming and cooling through the transition is 218 K, close to the warming T_1 value obtained from magnetic measurements (221 K). With the data density of the present study (a data point entry every 10 deg), no hysteresis effects were observed in the VTFTIR experiments, consistent with a continuous-type transition.

On cooling to 6 K, $Fe(phen)_2(NCS)_2$ and $Fe(5,6\text{-dmp})_2(NCS)_2$ appear to be fully converted to their LS forms, since only the LS ν_{CN} bands are observed, as shown in Figure 3b for $Fe(5,6\text{-dmp})_2(NCS)_2$. The small absorption at 2068 cm^{-1} is due to the ^{13}C component of the LS ν_{CN} band. The positions of the LS ν_{CN} bands for $Fe(phen)_2(NCS)_2$, $Fe(4,7\text{-dmp})_2(NCS)_2$,[13] and $Fe(5,6\text{-dmp})_2(NCS)_2$ are listed in Table IV.

(d) Mossbauer Studies. The ^{57}Fe Mossbauer spectra at 295 and 90 K of $Fe(5,6\text{-dmp})_2(NCS)_2$ (Figure 4) and $Fe(tmp)_2(NCS)_2$ (Figure 5) were obtained to compare the hyperfine parameters among the phenanthroline complexes. Mossbauer parameters of

all the complexes are shown in Table V. The room-temperature spectrum of $Fe(5,6\text{-dmp})_2(NCS)_2$ (Figure 4a), with a quadrupole splitting of 2.77 $mm\cdot s^{-1}$ and an isomer shift of 0.97 $mm\cdot s^{-1}$, shows that the HS form is the major phase. These values are in good agreement with those obtained by Bargeron and Drickamer (ΔE_q = 2.68 $mm\cdot s^{-1}$, δ^{IS} = 0.95 $mm\cdot s^{-1}$).[16] There is some evidence for an absorbance due to the LS form at 295 K, as magnetic susceptibility data predict, but the percentage of the LS form cannot be calculated accurately because of the low signal/noise ratio of the spectrum. The spectrum at 90 K (Figure 4b) shows that the complex is essentially completely converted to the LS form with ΔE_q = 0.44 $mm\cdot s^{-1}$ and δ^{IS} = 0.40 $mm\cdot s^{-1}$. The Mossbauer spectrum of $Fe(tmp)_2(NCS)_2$ (Figure 5 shows the 90 K spectrum) shows a single doublet at 295 and 90 K, which can be ascribed to HS iron(II).

(e) LIESST Studies. LS → HS_{tr} conversion (LIESST) studies on $Fe(5,6\text{-dmp})_2(NCS)_2$ show a number of similarities—as well as a number of differences—to the earlier optical pumping experiments reported for $Fe(phen)_2(NCS)_2$[6,7] and $Fe(4,7\text{-dmp})_2(NCS)_2$.[13] As with the earlier studies, fortuitous irradiation of the sample by the 0.5-mW He/Ne alignment laser resulted in measurable LS → HS_{tr} conversion, and hence, a blue filter was used to block this radiation.[6,7] White light irradiation at 6 K effected complete LS → HS_{tr} conversion in $Fe(phen)_2(NCS)_2$ and $Fe(4,7\text{-dmp})_2(NCS)_2$ within 20 min. The irradiation time needed to effect LS → HS_{tr} conversion in $Fe(5,6\text{-dmp})_2(NCS)_2$ varied among different mulls; some were completely converted upon white light irradiation, while others showed evidence of residual LS even after extended irradiation times. Figure 3c shows the CN stretching bands after the majority of the sample had been converted to the HS_{tr} form at 6 K. Variation in pumping behavior among different mulls of $Fe(5,6\text{-dmp})_2(NCS)_2$ may be related to the "dark relaxation" observed in this complex as discussed below.

After $Fe(5,6\text{-dmp})_2(NCS)_2$ was converted to the maximum attainable fraction of the HS_{tr} form with white light irradiation at 6 K, the sample was maintained at 6 K in the dark. After 1 h, a fraction of the HS_{tr} form had relaxed to the LS form. This dark relaxation was monitored at 6 K in two different mulls (A and B). Mull A was essentially fully converted to the HS_{tr} form with white light and showed 6% HS_{tr} → LS conversion after 1 h. Mull B could only be converted to 81% of the HS_{tr} form at 6 K and then showed a 16% conversion to the LS form after 1 h in the dark. A given mull did not show changes in this relaxation rate on going through several cycles of spin-state conversions. Since previous studies[3,9] have suggested that the rate of the HS → LS interconversion can be influenced by the LS fraction in the sample, a further experiment was performed to determine if the different rates for the $Fe(5,6\text{-dmp})_2(NCS)_2$ samples could be attributed to this type of effect. A third mull (C) was cooled to 6 K and converted to different percentages (41, 54, 69, and ~100%, in that order) of the HS_{tr} form. Subsequent dark relaxation was monitored in each case, and all showed a 3% HS_{tr} → LS conversion after 1 h. These results indicate that the different dark relaxation rates observed for $Fe(5,6\text{-dmp})_2(NCS)_2$ are not a consequence of varying amounts of residual LS present in each mull. Apparently, the dark relaxation is sensitive to some unknown variable which has not yet been controlled, although all three mulls were made in the same manner and from the same synthetic batch of $Fe(5,6\text{-dmp})_2(NCS)_2$. The different amounts of the residual LS form which cannot be pumped to the HS_{tr} form in different mulls are believed to be related to the steady-state balance between the conversion rates which are dependent on the white light irradiation (LIESST and reverse LIESST[9,31]) and those which proceed independent of light irradiation (the dark relaxation). If one of these rates is changed, the balance of states observed under steady-state conditions will be different (i.e. the amount of residual LS present at maximum pumping). VTFTIR measurements on other complexes,[10,13] which exhibit dark relaxation at low temperature, have shown that different intensity and/or irradiation source frequency on the same mull can produce different amounts of the HS_{tr} and LS forms under steady-state conditions.

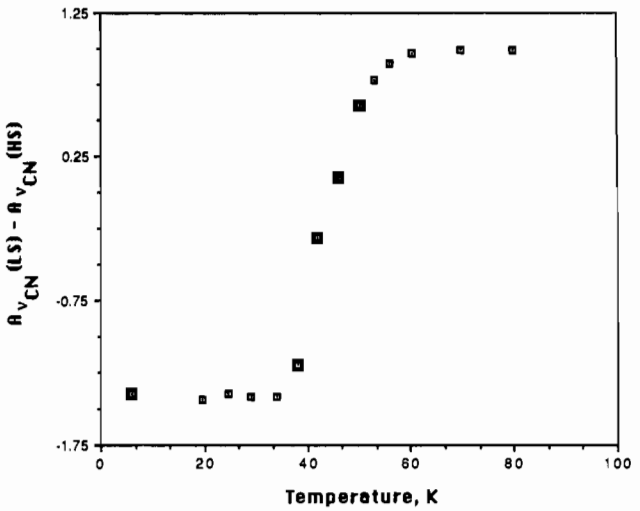

Figure 6. Maximum LS → HS_{tr} optical conversion as a function of temperature for $Fe(5,6\text{-dmp})_2(NCS)_2$. $A_{\nu CN}(LS) - A_{\nu CN}(HS)$ is the difference between the absorbance of the LS CN and HS CN stretching modes.

Unlike $Fe(5,6\text{-dmp})_2(NCS)_2$, $Fe(phen)_2(NCS)_2$ and $Fe(4,7\text{-dmp})_2(NCS)_2$, when cooled to 6 K and irradiated to yield ~100% of the HS_{tr} form, do not show any detectable relaxation to the LS form when maintained at 6 K in the dark and monitored over 1–2 h. The same experiment described above for $Fe(5,6\text{-dmp})_2(NCS)_2$ was performed on $Fe(phen)_2(NCS)_2$ to see if different amounts of residual LS would affect its rate of HS_{tr} → LS dark relaxation. It was found that $Fe(phen)_2(NCS)_2$ shows a dark relaxation at 6 K, which appears to be dependent on the amount of residual LS form present. When 100% of the HS_{tr} form was initially present, no conversion to the LS form was observed after 1 h; from initially 88% of the HS_{tr} form, a conversion of 2% was observed in 1 h, and from initially 48% of the HS_{tr} form, a conversion of 7% was observed in 1 h. In previous studies, these observations were accounted for using the lattice expansion model.[3,9] The volume difference between a HS and a LS molecule creates an image pressure throughout the lattice and slightly changes the potential energy of each form. Bargeron et al.[16] have demonstrated the pressure dependence of the HS → LS conversion at room temperature of $Fe(phen)_2(NCS)_2$, and some of the related complexes discussed here. The above experiment on $Fe(phen)_2(NCS)_2$ at 6 K demonstrates an increased HS → LS relaxation with increasing LS fraction, which agrees with Bargeron and Drickamer's results that increased pressure favors the LS form, as well as with the results predicted by the lattice expansion model.[3,9] The same experiment on $Fe(5,6\text{-dmp})_2(NCS)_2$ did not show a change in the HS_{tr} → LS relaxation rate dependent on the percent of LS present. Since the image pressure is proportional to the volume difference between the two states, it may be inferred that the volume change between HS and LS molecules in $Fe(5,6\text{-dmp})_2(NCS)_2$ is too small for its effects to be detected under the given experimental conditions.[8]

To elucidate the dynamics of low-T (<70 K) spin-state conversions in $Fe(5,6\text{-dmp})_2(NCS)_2$, the maximum amount of LIESST conversion was monitored as a function of temperature. In addition, at each temperature the HS_{tr} → LS change was followed as a function of time. By monitoring the optical conversion in the steady state, that is, spectra being taken while irradiation of the sample was in progress, it was possible to determine the maximum amount of HS_{tr} formed at each temperature. This quantity is plotted in Figure 6. These data serve to further characterize the LIESST phenomenon and permit a comparison between different complexes under identical experimental conditions.

After maximum conversion was reached at a given temperature, irradiation was stopped, and this point represented zero time for the subsequent determination of the dark relaxation rate. The rates at 19.5 and 24.5 K were equal to that at 6 K; i.e. in this range,

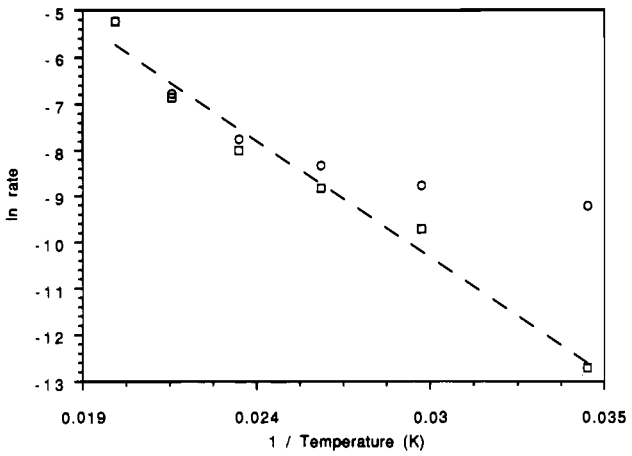

Figure 7. Arrhenius plot of the $HS_{tr} \rightarrow LS$ dark relaxation rates between 25 and 50 K for $Fe(5,6\text{-dmp})_2(NCS)_2$. The plot of ln k_{obs} vs $(\text{temperature})^{-1}$ is represented by the circles and the plot ln k_b vs $(\text{temperature})^{-1}$ is represented by the squares. The dashed line shows the linear fit of the ln k_b vs $(\text{temperature})^{-1}$ data ($R^2 = 0.988$).

the rate ($\sim 9 \times 10^{-5}$ s^{-1}) appears independent of temperature, suggesting that dark relaxation occurs via a tunneling mechanism. Between 29 and 50 K, on the other hand, the rate was temperature dependent, varying from 9.9×10^{-5} s^{-1} at 29 K to 5.4×10^{-3} s^{-1} at 50 K. Between 53 and 80 K, the rates were too rapid to permit accurate rate constants to be determined. An Arrhenius plot for the rates between 29 and 50 K is shown in Figure 7. The data points do not fall on a straight line, suggesting that $HS_{tr} \rightarrow LS$ conversion occurs by at least two pathways. If the second mechanism is assumed to be a classical energy barrier crossing, the observed relaxation rate (k_{obs}) can be set equal to the tunneling rate (k_t) plus the barrier crossing rate (k_b). If k_t is temperature independent, k_b can be calculated at each point between 29 and 50 K. An Arrhenius plot of ln k_b vs $1/T$ should give a straight line, and this is observed as shown in Figure 7. The best fit to a straight line was obtained using $k_t = 9.6 \times 10^{-5}$ s^{-1}, in agreement with the approximate value obtained for k_t at temperatures below 25 K. The activation energy calculated from the ln k_b vs $1/T$ plot is 4.0 kJ·mol^{-1}, comparable to those reported elsewhere.[8]

Conclusions. Several details of both the thermally and optically driven spin-state transitions in a series of complexes related to $Fe(phen)_2(NCS)_2$ via methyl substitution on the phenanthroline ligand have been examined. $Fe(5,6\text{-dmp})_2(NCS)_2$ has been shown through magnetic susceptibility, Mossbauer spectroscopy, and IR spectroscopy to undergo a relatively complete thermally-driven HS ⇔ LS transition. The transition appears to be of the continuous type with $T_1 = 221$ K. For the series studied, ligand field strength alone cannot explain the observed magnetic data, as has been shown in several other series of spin-crossover compounds.[30,31] The crystal structure of $Fe(2,9\text{-dmp})_2(NCS)_2 \cdot {}^1/_4H_2O$ has been determined, and shows evidence that steric hindrance is probably the reason this compound remains in the HS form down to 6 K.

The three complexes in the series which do undergo a thermally driven spin-state transition on cooling from room temperature [$Fe(phen)_2(NCS)_2$, $Fe(4,7\text{-dmp})_2(NCS)_2$, and $Fe(5,6\text{-dmp})_2(NCS)_2$] also demonstrate the LIESST phenomenon at liquid helium temperatures, with pseudo-first-order conversion rates. The first-order fit to these data indicates that the LIESST process involves a single chemical species, rather than cooperative, process.[10,32] In samples irradiated to yield ~100% of the HS_{tr} form, $Fe(5,6\text{-dmp})_2(NCS)_2$ relaxes to the LS form in the dark, whereas $Fe(phen)_2(NCS)_2$ and $Fe(4,7\text{-dmp})_2(NCS)_2$ do not. This basic difference between the continuous and discontinuous spin-crossover compounds has been observed in other systems studied in this laboratory.[13] The relaxation of $Fe(phen)_2(NCS)_2$ at 6 K after partial conversion to the HS_{tr} form is believed to be a pressure-induced phenomenon (image pressure[21]) and therefore different from the dark relaxation observed when a continuous-type complex is converted to ~100% HS_{tr} at 6 K. The variable-temperature rates obtained for the $HS_{tr} \rightarrow LS$ dark relaxation in $Fe(5,6\text{-dmp})_2(NCS)_2$ provide evidence of two mechanisms. At temperatures below ~25 K it appears that tunneling is the dominant relaxation mechanism. As the temperature is increased, classical energy barrier crossing becomes dominant with an activation energy of ~4 kJ·mol^{-1}. There are now several examples of spin-crossover compounds in which tunneling appears to be a mechanism for either the thermally-driven spin-crossover transition or the $HS_{tr} \rightarrow LS$ relaxation (dark relaxation).[8,11,33,34]

The previous $HS_{tr} \rightarrow LS$ relaxation data of Hauser et al.[9] were obtained from temperature-jump experiments. The relaxation was monitored at temperatures above ~50 K, and therefore these results probably reflect classical energy barrier crossing rates. These relaxations were found to be cooperative in nature, and as a result, the rate plots were more sigmoidal in shape and did not fit well to a first-order rate law. Cooperative effects in the $Fe(5,6\text{-dmp})_2(NCS)_2$ dark relaxation appear to be minimal, providing consistent evidence for the two mechanisms of the $HS_{tr} \rightarrow LS$ conversion in this complex. Several other attempts, by the present investigators, to monitor and account for the details of $HS_{tr} \rightarrow LS$ relaxation in the low temperature regime in other complexes have shown this phenomenon to be complex, presumably due to cooperative and/or cycling effects.

Acknowledgment. We acknowledge with sincere thanks the Hebrew University Nuclear Physics group for help in acquiring the Mossbauer data, Prof. M. Greenblatt and members of her group (especially K. V. Ramanujachary) at Rutgers University for acquisition of the magnetic data, and Prof. H. Schugar for acquiring the single-crystal data on $Fe(2,9\text{-dmp})_2(NCS)_2 \cdot {}^1/_4H_2O$. Funds for the instrumentation used in this study were provided from the following grants: NSF DMR 810 2940, NIH 87-0208, and Instrumentation Grant 1510 RRO 1486 01A1. D.C.F. acknowledges financial support in the form of a Patricia Harris Fellowship.

Supplementary Material Available: Tables of H and O atom parameters, bond angles, least-squares planes, anisotropic thermal parameters, and crystal and refinement data (10 pages); a listing of observed and calculated structure factors (13 pages). Ordering information is given on any current masthead page.

(30) (a) Klaui, W.; Eberspach, W.; Gutlich, P. *Inorg. Chem.* **1987**, *26*, 3977. (b) Goodwin, H. A.; Mather, D. W. *Aust. J. Chem.* **1974**, *27*, 2121. (c) *Ibid.* **1974**, *27*, 965.
(31) Gutlich, P.; Hauser, A. *Coord. Chem. Rev.* **1990**, *97*, 1.
(32) Hauser, A. *Chem. Phys. Lett.* **1986**, *124*, 543.
(33) (a) Xie, C.-L.; Hendrickson, D. N. *J. Am. Chem. Soc.* **1987**, *109*, 6981. (b) Conti, A. J.; Xie, C.-L.; Hendrickson, D. N. *J. Am. Chem. Soc.* **1989**, *111*, 1171.
(34) Alder, P.; Poganiuch, P.; Spiering, H. *Hyperfine Interact.* **1989**, *52*, 47.
(35) Konig, E.; Madeja, K. *Inorg. Chem.* **1967**, *6* (1), 48.